# Low-threshold epitaxially grown 1.3 μm InAs quantum dot lasers on patterned (001) Si

Chen Shang, Yating Wan, Justin Norman, Noelle Collins, Ian MacFarlane, Mario Dumont, Songtao Liu, Qiang Li, Kei May Lau, Arthur C. Gossard, John E. Bowers

***Abstract*—A three-fold reduction of threshold current, with a minimum threshold current density of 286 A/cm$^2$, a maximum operating temperature of 80 °C, and a maximum 3 dB bandwidth of 5.8 GHz was achieved for 1.3 μm InAs quantum dot lasers on patterned, on-axis (001) Si. This was enabled by the reduced threading dislocation density (from 7×10$^7$ to 3×10$^6$ cm$^{-2}$), and optimized probe design. The patterned Si produced antiphase domain free material in the coalesced GaAs buffer layer with reduced misfit/threading dislocation nucleation, without the use of Ge/GaP buffers or substrate miscut. Utilizing aspect ratio trapping, cyclic thermal annealing, and dislocation filter layers, high quality III-V on Si devices were grown, demonstrating the compelling advantages of this patterned Si template for a monolithic Si photonics integration platform.**

***Index Terms*— Integrated optoelectronics, quantum dots, wafer scale integration**

## I. Introduction

The explosive growth of Internet Protocol (IP) traffic is driving data centers into the Zettabyte Era. Consuming 1.5% of the total energy consumed in the U.S. at a cost of $4.5B, the data centers' energy consumption is predicted to triple by 2020 [1]. Today, Si photonics supplies 100% of the 80 km dense wavelength division multiplexing (DWDM), >75% of the parallel single mode 4-channel (PSM4), and >50% of the 2 km coarse 4 × 25 Gbps coarse wavelength division multiplexing (CWDM4) for Microsoft [2]. This technology is currently fueling high bandwidth density interconnection links and is primed to serve other growth markets such as light detection and ranging (LIDAR) and chip-scale wearable sensors [3]. Although Si-based light guiding, modulation and detection technologies have been explored extensively with impressive achievements [4], the indirect bandgap has hampered the development of an on-chip light source.

Recently, InAs quantum dots (QDs) have demonstrated themselves as the most promising candidate for achieving high performance light emitters epitaxially grown on Si [5-12]. The effective carrier localization in QDs considerably improves laser reliability over quantum well (QW) lasers on Si by suppressing growth of ⟨1 1 0⟩ dark-line defects [14]. The extrapolated mean time to failure, as defined by doubling of the initial threshold current, are now more than 10,000,000 hours for state-of-art QD lasers on Si at 35 °C [15]. In contrast, the most prolonged lifetime reported among GaAs-based QW lasers on Si is merely ~200 h after more than a decade of research [16].

To date, intensive research has been conducted to migrate this field to the use of complementary metal–oxide–semiconductor (CMOS) compatible on-axis Si substrates [17-21]. Various novel methods have been applied to solve the anti-phase domain (APD) problem, obviating the need for miscut substrates. These approaches range from direct nucleation of a GaAs film with special Si wafer preparation [17, 18], growing an $Al_{0.3}Ga_{0.7}As$ seed layer [19], the use of a thin GaP buffer layer [15], 0.15° misorientation in the [110] direction [20], U-shaped patterned Si (001) substrates to obtain (111)-faceted-sawtooth Si hollow structures [21], and patterned growth on exposed {111} V-groove facets of silicon [22]. Leveraging the aspect ratio trapping effects, we previously demonstrated electrically injected QD lasers grown on on-axis (001) Si with {111} V-groove facets [23]. The "tiara"-like structures formed by the patterned Si simultaneously circumvent the issue of APDs and effectively filter out stacking faults in the coalesced GaAs buffer layer without additional Ge/GaP buffers or substrate miscut [24]. A comprehensive comparison of the lasing characteristics in devices with the same active structure and geometry but fabricated on this V-groove Si template in conjunction with our simultaneously developed GaP/Si template has been made [25]. Despite the fact that the GaP/Si possesses three-fold lower defect densities, devices on V-groove Si substrate achieved continuous-wave (CW) lasing with thresholds as low as 36 mA for a 6×1200 μm$^2$ ridge laser with 95% reflectivity coating on one facet [23] and submilliamp threshold of 0.6 mA for a microring laser with an outer radius of 5 μm and a ring width of 3 μm [12]. Furthermore, the V-

Manuscript received January 30, 2019. This work was supported by Advanced Research Projects Agency-Energy (ARPA-E), No 16212115; the American Institute for Manufacturing – Integrated Photonics, DE-AR0000672. Research Grants Council of Hong Kong (RGC) and Innovation Technology Fund of Hong Kong (ITS/320/14).

C. Shang, J. C. Norman, and A. C. Gossard are with the Materials Department, University of California, Santa Barbara, CA 93106 USA (e-mail: shang00@umail.ucsb.edu; jnorman@ucsb.edul; acgossard@gmail.com).

Y. Wan, S. Liu, and J. E. Bowers are with the Institute for Energy Efficiency, University of California, Santa Barbara, CA 93106 USA (e-mail: yatingwan@ucsb.edu; stliu@ece.ucsb.edu; bowers@ece.ucsb.edu).

N. Collins, I. MacFarlane, M. Dumont are with the Department of Electrical and Computer Engineering, University of California, Santa Barbara, CA 93106 USA (e-mail: noellecollins@ucsb.edu; ian@macfarlanehome.com; mariodumont@ucsb.edu).

Q. Li, K. M. Lau are with Department of Electronic and Computer Engineering, Hong Kong University of Science & Technology, Clear Water Bay, Hong Kong (e-mail: (e-mail: qli@connect.ust.hk; eekmlau@ust.hk).

C. Shang, Y. Wan, and J. C. Norman contribute equally in this manuscript. (Corresponding author: Yating Wan, yatingwan@ucsb.edu)

.

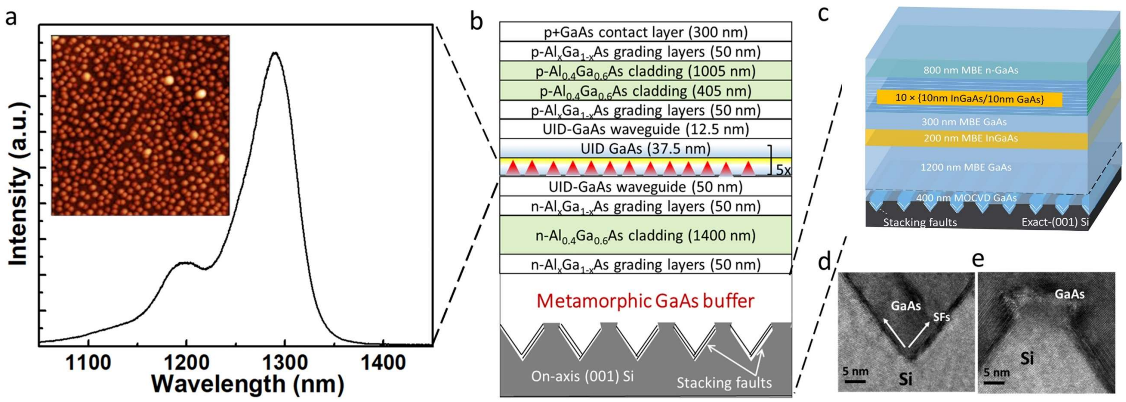


Fig. 1. (a) Photoluminescence spectrum of the as-grown sample. Inset: atomic force microscopy image of QD with a density of $6.4\times 10^{10}$ cm$^{-2}$. The image has a size of $1 \times 1$ μm$^2$. (b) The full stack of the laser structure. (c) Schematic image of the buffer structure. Materials above the dashed line are grown by MBE. (d) and (e) Cross-sectional TEM images of the V-grooved structure, showing stacking faults (indicated by the white arrows) trapped by the Si pockets.

groove Si is advantageous in providing a smoother surface and thinner buffer layers which saves growth time, and is beneficial for subsequent device fabrication [26].

Here, by combining the additional effects of thermal cyclic annealing and strained-layer superlattices, a record-low threading dislocation density (TDD) of $3\times10^6$ cm$^{-2}$ on a V-groove Si template was achieved. This is more than a 20-fold reduction over the previously reported TDD on V-groove Si [22], half of the value in the state-of-art GaP/Si template [10], and closes the gap relative to the best reported dislocation densities for lasers on Si [7, 20]. The significant decrement of TDD translates into a three-fold reduction of threshold currents (minimum value of 12 mA here, while the value is 36 mA in [22]), with a minimum threshold current density of 286 A/cm$^2$, and a maximum operating temperature of 80 °C. Furthermore, by optimizing the probe design, a maximum 3 dB bandwidth of 5.8 GHz was achieved. This is larger than the theoretically predicted modulation bandwidth maximum (of 5GHz) in a recent report of monolithic 1.3 µm InAs/GaAs QD lasers on Si [27].

## II. Experimental Procedure

The GaAs-on-v-groove Si template, shown in Fig. 1(c), was grown by the combined effort of both metal-organic chemical vapor deposition [23] (the first 400 nm coalesced GaAs) and solid-source molecular beam epitaxy (MBE). The GaAs nanowires were first selectively grown in the V-grooves, with openings of 70 nm, of the patterned (001) Si wafer on {111} planes. The $SiO_2$ stripes were then removed using buffered oxide etch (BOE). The GaAs nanowires coalesced into a continuous thin film after growing to a total thickness of 100 nm at 600 ºC. Then, 300 nm of additional GaAs was deposited for planarization. Stacking faults nucleated at the GaAs-Si interface accommodate for the 4.1% lattice mismatch, which were then blocked by the Si ridges and thereby contained in the V-grooves. The high index growth plane ensured that no APDs would form at the interface. It is worth to mentioning that there is more than one strain relaxation mechanism for V-groove epitaxy under different growth parameters [28]. The result from IMEC [29] shows the relaxation of III/V on {111} facets based on misfit and TD formation.

Here, by making use of a different strain relaxation mechanism (compared to blanket epitaxy in [16-18]) based on a highly twinned region with thickness <10 nm, the tip of the Si ridges ensures the stress-relaxing layer is confined within the V-shaped trenches. This phenomenon is shown in the cross-section bright-field transmission electron microscopy (TEM) image in Fig. 1(d) and (e). Thus, the V-groove approach eliminates APDs and moderately reduces TDD, while the main defect reduction was realized through the remaining structure of the GaAs-on-Si buffer by MBE [22]. In the MBE buffer, four cycles of temperature annealing from 400 °C to 700 °C were applied after the initial 1200 nm GaAs growth, which provides additional kinetic energy for the TDs to increase their in-plane movement and promotes them to meet and annihilate. Next, 200 nm of $In_{0.1}Ga_{0.9}As$ and ten periods of $In_{0.1}Ga_{0.9}As$/GaAs (10 nm/10 nm) superlattices were employed to promote lateral movement of the TDs through the induced compressive stress. The buffer structure was finished with 800 nm *n*-doped GaAs with a concentration of $2\times10^{18}$ cm$^{-3}$. A root-mean-square roughness of ~2.8 nm was obtained across a scanning area of $5\times5$ µm$^2$ in the atomic force microscopy (AFM) image, shown in Fig. 2(a). The final TDD was measured to be $3 \times 10^6$ cm$^{-2}$ by electron channeling contrast imaging (ECCI) shown in Fig. 2(b).

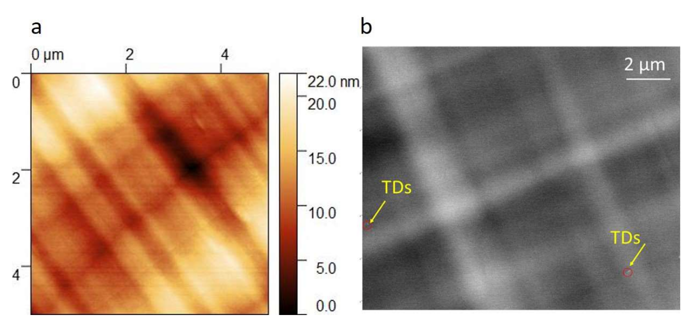


Fig. 2. (a) AFM and (b) ECCI of the buffer structure. In the AFM, a root-mean-square roughness of ~2.7 nm was obtained across a scanning area of $5\times5$ µm$^2$. The vertical bar is 22 nm. In the ECCI, TDD is as low as $3 \times 10^6$ cm$^{-2}$. The circles show the only threads in the image.

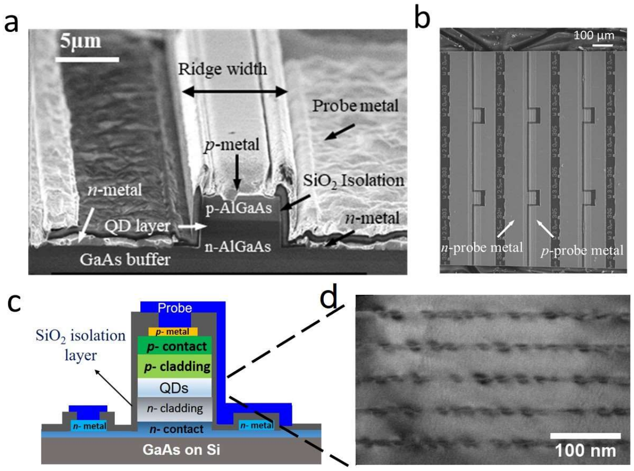


Fig. 3. (a) SEM image of the cross-section of an as-cleaved laser, tilted at 75º. (b) Schematic image of the laser cross-section, revealing the geometry of the contact and probe metals. (c) Top-down view of the laser bar. Each tick mark on the metal pad indicates a length of 100 µm. (d) Bright-field TEM image of the active region cross-section, showing the five layers of QDs.

The full laser structure with 5 layers of QD as the active region was grown on top of the buffer structure, as shown in Fig. 1(b). A GaAs/AlGaAs graded-index separate confinement heterostructure was used as the cladding layer for both optical and electrical confinement. Fig. 1(a) shows the room temperature photoluminescence (PL) spectrum of the InAs QDs, which has a peak intensity around 1290 nm for the ground-state transition and a full width at half maximum of about 30 meV. The nominal InAs thickness was 2.75 ML. The optimized growth temperature was 495 °C under $As_4$ overpressure at a V/III of 35. The dots were grown in an $In_{0.15}Ga_{0.85}As$ well with 2 nm below and 5 nm capping the dots followed by a 2.5 nm GaAs layer. The "In-flush" technique was employed at 580°C to improve dot uniformity [30]. The bottom cladding layers were grown at 580 °C while the growth temperature for the top cladding layers was lowered to 560 °C to reduce the QD intermixing. All temperatures were measured by pyrometer. The inset of Fig. 1(a) is the AFM image of the as grown dots, showing that the areal density of the dots is about $6.4 \times 10^{10}$ $cm^{-2}$.

Fig. 3 summarizes the structure of the as-fabricated laser devices. Fig. 3(a) and (b) show the SEM and schematic image of the laser cross-section, respectively. The laser ridges were formed perpendicular to the V-grooves by inductively coupled plasma (ICP) etching down to the *n*-contact layer. Laser facets were formed by cleaving, with cavity lengths of 750, 1450, and 2000 µm and ridge widths ranging from 1 to 10 µm. Fig. 3(c) shows the top-down view of the as-cleaved laser bars. Sidewall scattering and surface recombination can be significant problems for the deeply etched devices. Thus, after ridge mesa formation, 12 nm of $Al_2O_3$ was applied by atomic-layer deposition (ALD) to passivate the side wall. An 800 nm thick $SiO_2$ layer was then deposited by sputtering for electrical isolation and to isolate the optical modes from the Pd/Ti/Pd/Au (*p*) and Pd/Ge/Pd/Au (*n*) metal contact layers. The five layers of QDs are clearly visible in the cross-section bright-field TEM image in Fig. 3(d), taken with g = (002) under two beam condition. The individual dots revealed themselves as dark spots in the TEM image as they distort the surrounding lattice locally.

## III. RESULTS AND DISCUSSION

110 ridge lasers were tested at room temperature under CW operation. Fig. 4(a) shows the typical light–current–voltage (LIV) characteristics of a laser with a 1450 µm cavity length and 10 µm ridge width. The measured 1 V turn-on voltage and 2.7 Ω differential series resistance from the I-V curve indicate good metal contacts for efficient current injection. A clear knee behavior in the LI curve is observed at the lasing threshold current of 39 mA. This corresponds to a threshold current density ($J_{th}$) of 270 A/$cm^2$, or 54 A/$cm^2$ per QD layer. No output saturation was observed when the output power reached 75 mW per facet at an injection current of 600 mA, which corresponds to a total output power exceeding 150 mW assuming equal output from both facets. Power roll over occurs until the injection reaches 650 mA. A maximum wall-plug efficiency of 15.6% was achieved. As a comparison, in Fig. 4(b), for a laser with the same cavity length of 1450 µm, but a smaller ridge width of 2 µm, the maximum power of 33 mW per facet is obtained at an injection current of 318 mA, with a threshold current of 16 mA.

Figure 5 depicts a threshold current density histogram for all measured lasers, with the peak located around 400 to 500 A/$cm^2$ and a minimum of 270 A/$cm^2$. As a comparison, our previously reported lasers on the V-groove Si template had a threshold current density distribution peaked around 700 to 1000 A/$cm^2$. The main difference between the two is the threading dislocation density at the surface of the buffer. The inset of Fig. 5 shows a continuously decreasing trend of threshold current as the ridge width narrows down to 1.5 µm. This suggests that the side wall recombination is greatly suppressed by the well-

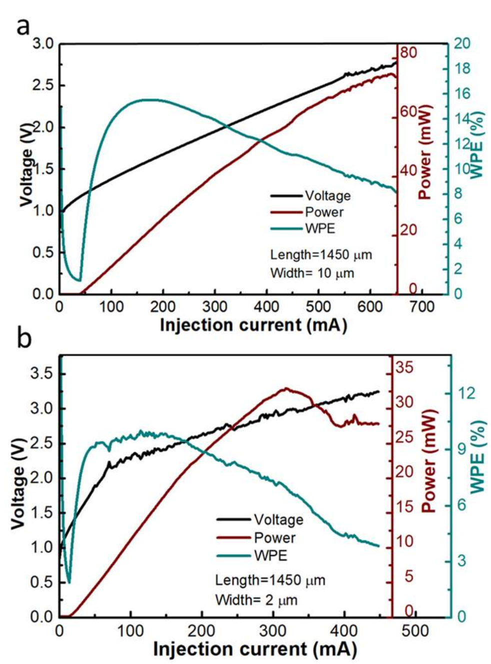


Fig. 4. Typical L-I-V characteristics of an as-cleaved laser with a cavity length of 1450 µm and a ridge width of (a) 10 µm and (b) 2 µm, together with the wall-plug efficiency.

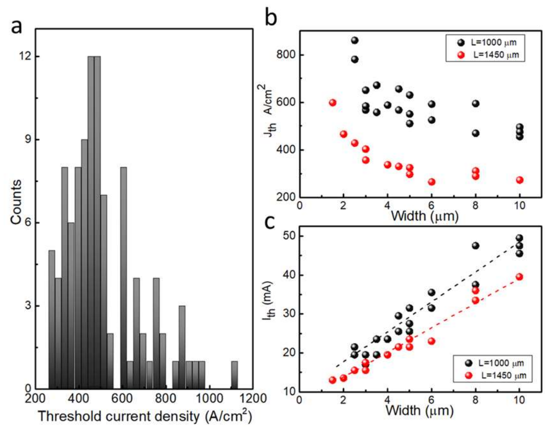

Fig. 5. Threshold current density distribution histogram for all measured lasers. Most of the devices fall between 300 and 500 A/cm$^2$. The inset shows a continuous decrease of threshold current with reduced ridge width, indicating good suppression of side-wall recombination.

optimized $Al_2O_3$ passivation layer as well as the reduced carrier diffusion length from the QD active region. The higher threshold current with shorter cavities is due to the increase in the mirror loss. The typical carrier diffusion length of a QW active region is about 3 to 5 µm, and this value is reduced to about 1 µm with the QD active region [31]. The reduced carrier diffusion length is the reason for QD's insensitivity to internal defects as well as device side walls.

The spectra of a device with 1450 µm cavity length and 2 µm ridge width are shown in Fig. 6. The primary lasing peaking is located around 1284 nm. A slight red-shift of the lasing wavelength with increasing injection current was observed. It was interesting to notice that at low injection levels, namely less than 35 mA, an apparent single mode operation was obtained with side-mode-suppression ratio of about 35 dB. There was a crack perpendicular to the ridge direction, suggesting that the realization of single-mode operation is due to the laser effectively operating as a coupled-cavity device with large cavity length ratio [32]. The inset of Fig. 6 shows the measured laser linewidth is about 14 MHz using self-heterodyne method.

We also tested the same device at elevated temperatures as shown in Fig. 7. The laser was able to function under CW operation up to 80 °C for ground state lasing, still producing an output power of ~4 mW. This demonstrates that the QD lasers on the V-groove Si template can meet the temperature

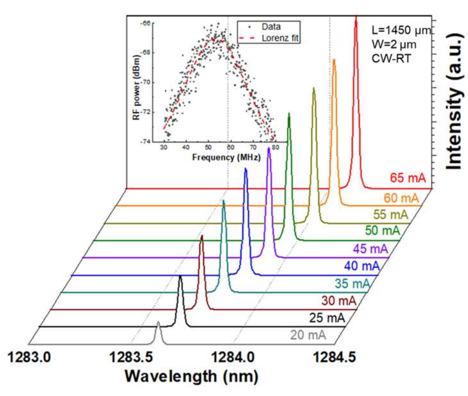

Fig. 6. Lasing spectra of a device with 2×1450 µm$^2$ cavity. The primary lasing peak is located around 1284 nm. Single-mode operation was observed below 35 mA bias current. Inset: measured laser linewidth using self-heterodyne method.

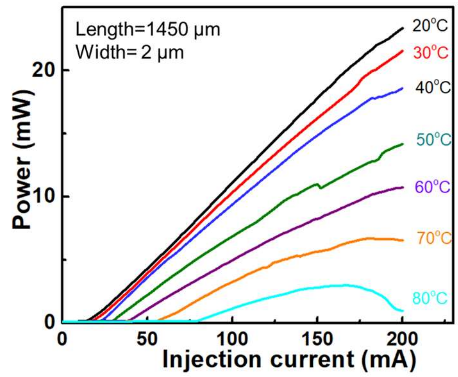

Fig. 7. High temperature measurements of the same device show lasing up to 80 °C under CW operation.

requirement in a realistic datacenter environment. This result compares favorably to the best heterogeneously integrated quantum dot lasers on Si which operate CW up to 100°C [33].

The natural logarithm of threshold current versus stage temperature for the ridge laser in Fig. 7 and other lasers with the same length but different widths are plotted in Fig. 8. Using an exponential function of $P_{th} \propto \exp\left(\frac{T}{T_0}\right)$, the characteristic temperature $T_0$ was extracted to fall into the range of 30-35 K, as shown in the inset of Fig. 8. Even though lasers with narrower ridges have smaller heat extraction area through the bottom Si to the heat sink, they are as insensitive, if not more, to temperature change as the lasers with wider ridges. There are two possible reasons. Firstly, a considerable amount of heat was extracted from the side walls, where narrower lasers had advantages with their higher area to volume ratio. Secondly, the residual thermal stress in GaAs on Si (~250 MPa) could be relieved with the higher aspect-ratio laser structures [34]. Fig. 9 depicts the small-signal modulation response, $S_{21}$, of type A laser and type B laser with the same dimension (length of 1450 µm and a width of 5 µm) biased from 24 to 88 mA, respectively. For the type A laser in Fig. 9(a), the probe metals were designed in a way that there was no vertical overlap between the *p*- and *n*- contact metal due to the cross-over of *p n* probe metal. This is contrary to that of the type B laser in Fig. 9(b), where a portion of *p*-probe was placed upon the *n*-metal area with an 800 nm $SiO_2$ separation layer. Otherwise, the two structures are

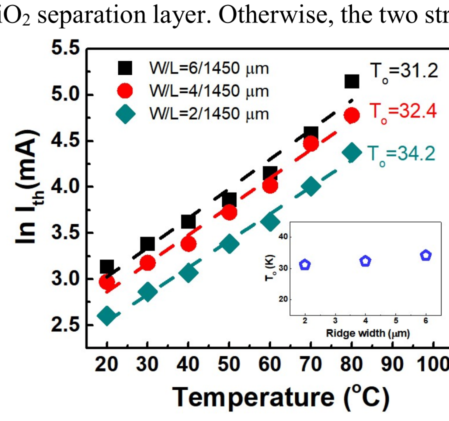

Fig. 8. Natural logarithm of threshold current versus stage temperature for ridge lasers with various width and a constant length of 1450 µm. The dashed lines represent linear fitting to the experimental data. Inset: the corresponding characteristic temperature as a function of the ridge width, which shows narrowing of the laser ridge does not increase the temperature sensitivity of the threshold current.

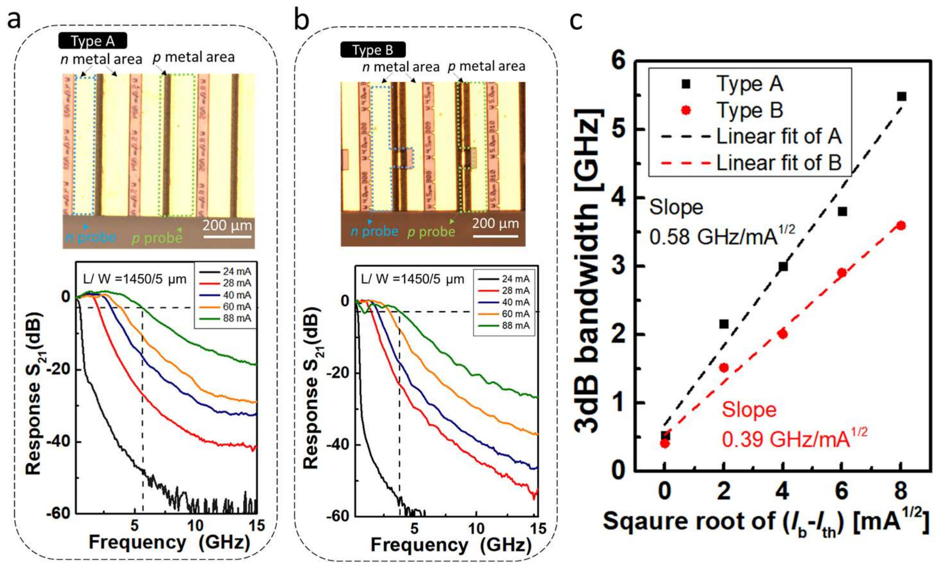


Fig. 9. Frequency response of a (a) type A laser and (b) type B laser with the same dimension (length of 1450 µm and a width of 5 µm) biased from 24 to 88 mA. The maximum $f_{3dB}$ saturated at 5.8 GHz for type A laser and 3.6 GHz for type B laser. The upper inset shows the microscopic image of the corresponding laser. (c) 3dB bandwidth versus square root of the bias current above threshold of the two types of laser in (a) and (b) The dashed lines represent linear fitting to the experimental data.

nominally the same in terms if epi structure and device fabrication. The 3 dB bandwidth, $f_{3dB}$, increased with increasing bias current and saturated at 5.8 GHz for type A laser and 3.6 GHz for type B laser when biased at 88 mA. The measurement procedure was similar to that described in [35]. The inset in Fig. 9 shows the plots of $f_{3dB}$ as a function of square root of bias current above threshold. The modulation efficiencies of $f_{3dB}$ for type A laser and type B laser are 0.58 GHz/mA$^{1/2}$ and 0.39 GHz/mA$^{1/2}$. The reduced parasitic capacitance of type A laser gives rise to a decent $f_{3dB}$ similar to that measured from the state-of-art result (6.5 GHz $f_{3dB}$ and 0.58 GHz/mA$^{1/2}$ modulation efficiency) on GaP/Si where 8 pairs of $SiO_2$/$Ta_2O_5$ films are coated on one facet to achieve a low mirror loss (99% reflection) and allow for lasing in small cavities (cavity length of 580 µm and ridge width of 3 µm) [35]. Note that the device presented here has a much longer length of 1450 µm and a width of 5 µm, with both facets formed as cleaved. As a comparison, the recent reported maximum 3dB bandwidths and modulation current efficiency of QD laser grown on Si with as-cleaved facet is only 1.6 GHz and 0.4 GHz/mA$^{1/2}$ (cavity length of 2500 µm and ridge width of 2.2 µm) [36]. With an optimized QD laser design readily based on the current growth process by scaling the number of QD layers and the cavity length, their modelling suggests that theoretical modulation bandwidth is only 5 GHz [27].

## IV. Conclusion

In conclusion, we report a significant improvement of QD laser performance grown on V-grooved Si. The utilization of $In_{0.1}Ga_{0.9}As$ strained layers and cycles of temperature annealing reduces the TDD from $7\times10^7$ to $3\times10^6$ cm$^{-2}$. This translates into a reduced minimum threshold current density from ~700 A/cm$^2$ to ~286 A/cm$^2$, with minimum threshold current of 12 mA and a maximum operating temperature of 80 °C. By optimizing the probe design, a maximum 3 dB bandwidth of 5.8 GHz has been achieved, which exceeds the previous theoretical prediction of modulation bandwidth [27]. Commercial use will require stable long-term operation above room temperature without an additional active cooling system. It has been reported that the main cause of device failure during prolonged operation is the growth of dislocation networks in the laser material [37]. Despite the QD's insensitivity to defects, the in-plane misfit dislocations interacting with multiple QDs in a row can be detrimental to device performance. Such misfit dislocations are thought to nucleate from existing TDs. Since reducing the number of TDs can effectively increase the energy barrier to nucleate misfit dislocations [38], lasers grown on GaAs-on-Si buffer with lower TDD are expected to possess higher reliability during device operation. According to the investigation of the impact of threading dislocation density on the reliability [39], reducing the dislocation density from $2.8\times10^8$ to $7.3\times10^6$ cm$^{-2}$ has improved the laser lifetime from a few thousand hours to more than $10\times10^6$ h at 35 °C and at twice the threshold current density. With the record low TDD ($3\times10^6$ cm$^{-2}$) buffer on patterned Si, one can envision further improved lifetime.

## Acknowledgment

We are grateful to UCSB nanofabrication clean room staff for helpful discussions and assistance.

## References

[1] Cisco Visual Networking, "The Zettabyte Era–Trends and Analysis," Cisco white paper (2017)

[2] Workshop at executive forum 208 by Jamie Gaudette (Microsoft).

[3] J. E. Bowers, and A. Y. Liu, (2017, March). A comparison of four approaches to photonic integration. In Optical Fiber Communication Conference (pp. M2B-4). Optical Society of America.

[4] T. Komljenovic, et al., "Photonics Integrated Circuits Using Heterogeneous Integration on Silicon." Proceedings of the IEEE, vol 106, No. 12, pp 2246-2257

[5] K. Nishi, K. Takemasa, M. Sugawara, and Y. Arakawa, "Development of quantum dot lasers for data-com and silicon photonics applications," *IEEE Journal of Selected Topics in Quantum Electronics,* vol. 23, no. 6, pp. 1-7, 2017.

[6] D. Bimberg and U. W. Pohl, "Quantum dots: promises and accomplishments," Materials Today, vol. 14, no. 9, pp. 388-397, 2011.

[7] Z. I. Kazi, T. Egawa, T. Jimbo, and M. Umeno, "First room-temperature continuous-wave operation of self-formed InGaAs quantum dot-like laser on Si substrate grown by metalorganic chemical vapor deposition," Jpn. J. Appl. Phys., vol. 39, no. 7R, 2000, Art. no. 3860

[8] S. Chen, et al., "Electrically pumped continuous-wave III–V quantum dot lasers on silicon," Nature Photon., vol. 10, pp. 307–311, 2016.

[9] Y. Wang, et al., "Electrically-pumped continuous-wave quantum-dot distributed feedback laser array on silicon," Optica 5.5, pp. 528–533, 2018.

[10] J. C. Norman, D. Jung, Y. Wan, and J. E. Bowers, "Perspective: The future of quantum dot photonic integrated circuits," APL Photon., vol. 3, no. 3, 2018, Art. no. 030901.

[11] D. Jung, et al., "High efficiency low threshold current 1.3 μm InAs quantum dot lasers on on-axis (001) GaP/Si," Appl. Phys. Lett., vol. 111, no. 12, 2017, Art. no. 122107.

[12] Y. Wan, et al., "1.3 μm submilliamp threshold quantum dot micro-lasers on Si," Optica, vol. 4, no. 8, pp. 940–944, Aug. 2017.

[13] S. Liu, et al., "High-channel-count low-noise 20 GHz passively mode locked quantum dot laser directly grown on Si with 4.1 Tbit/s transmission capacity," Optica, 6(2), 2019.

[14] R. W. Herrick et al., "Reliability of quantum well and quantum dot lasers for silicon photonics (invited)," in Proc. IEEE Photon. Conf., 2017, p. 11

[15] D. Jung, et al., "Highly reliable low threshold InAs quantum dot lasers on on-axis (001) Si with 87% injection efficiency," ACS Photon., vol. 5, no. 3, pp. 1094–1100, 2018.

[16] Z. I. Kazi, P. Thilakan, T. Egawa, M. Umeno, and T. Jimbo, "Realization of GaAs/AlGaAs lasers on Si using epitaxial lateral overgrowth by metalorganic chemical vapor deposition," Jpn. J. Appl. Phys., vol. 40, pp. 4903–4906, 2001.

[17] K. Li, et al. "O-band InAs/GaAs quantum dot laser monolithically integrated on exact (0 0 1) Si substrate." Journal of Crystal Growth 511 (2019): 56-60.

[18] Y. Wang, et al. "Three-step growth of metamorphic GaAs on Si (001) by low-pressure metal organic chemical vapor deposition." Journal of Vacuum Science & Technology B, Nanotechnology and Microelectronics: Materials, Processing, Measurement, and Phenomena 31.5 (2013): 051211.

[19] J. Kwoen, Jinkwan, et al. "All MBE grown InAs/GaAs quantum dot lasers on on-axis Si (001)." *Optics express* 26.9 (2018): 11568-11576.

[20] R. Alcotte, et al., "Epitaxial growth of antiphase boundary free GaAs layer on 300 mm Si (001) substrate by metalorganic chemical vapour deposition with high mobility," *APL Materials,* vol. 4, no. 4, p. 046101, 2016.

[21] W.-Q. Wei, et al., "InAs QDs on (111)-faceted Si (001) hollow substrates with strong emission at 1300 nm and 1550 nm," Applied Physics Letters, vol. 113, no. 5, p. 053107, 2018.

[22] Y. Wan, et al., "Optically pumped 1.3μm room-temperature InAs quantumdot micro-disk lasers directly grown on (001) silicon," Opt. Lett., vol. 41, pp. 1664–1667, 2016.

[23] J. Norman, et al., "Electrically pumped continuous wave quantum dot lasers epitaxially grown on patterned, on-axis (001) Si," Opt. Exp., vol. 25, no. 4, pp. 3927–3934, 2017.

[24] Q. Li, K. W. Ng, and K. M. Lau, "Growing antiphase-domain-free GaAs thin films out of highly ordered planar nanowire arrays on exact (001) silicon," Appl. Phys. Lett., vol. 106, p. 072105, 2015.

[25] Y. Wan, et al., "O-band electrically injected quantum dot micro-ring lasers on on-axis (001) GaP/Si and V-groove Si," Opt. Express, vol. 25, pp. 26853–26860, 2017

[26] Y. Wan, et al., "Sub-wavelength InAs quantum dot micro-disk lasers epitaxially grown on exact Si (001) substrates," Appl. Phys. Lett., vol. 108, p. 221101, 2016.

[27] C. Hantschmann, et al., " Small-Signal Modulation and Analysis of Monolithic 1.3 μm InAs/GaAs Quantum Dot Lasers on Silicon." 2018 European Conference on Optical Communication (ECOC). IEEE, 2018.

[28] Kunert, Bernardette, et al., "How to control defect formation in monolithic III/V hetero-epitaxy on (100) Si? A critical review on current approaches." Semiconductor Science and Technology 33.9 (2018): 093002.

[29] Shi, Yuting, et al., "Optical pumped InGaAs/GaAs nano-ridge laser epitaxially grown on a standard 300-mm Si wafer." Optica 4.12 (2017): 1468-1473.

[30] S. Haffouz, et al., "Growth and fabrication of quantum dots superluminescent diodes using the indium-flush technique: A new approach in controlling the bandwidth" Journal of Crystal Growth, 311, pp.1803-1806, 2009

[31] S. A. Moore, et al., "Reduced surface sidewall recombination and diffusion in quantum-dot lasers." IEEE photonics technology letters 18.17 (2006): 1861-1863.

[32] J. Bowers, et al., "Cleaved-coupled-cavity lasers with large cavity length ratios for enhanced stability" Appl. Phys. Letter., vol. 44, p. 82, 1984

[33] G. Kurczveil, D. Liang, M. Fiorentino, and R. G. Beausoleil, "Robust hybrid quantum dot laser for integrated silicon photonics," Opt. Express 24(14), 16167–16174 (2016).

[34] Vega-Flick, Alejandro, et al., "Reduced thermal conductivity of epitaxial GaAs on Si due to symmetry-breaking biaxial strain." arXiv preprint arXiv:1901.03455 (2019).

[35] D. Inoue, et al., "Directly modulated 13 μm quantum dot lasers epitaxially grown on silicon," Opt. Express, vol. 26, no. 6 pp. 7022-7033, 2018.

[36] Hantschmann, Constanze, et al., "Understanding the Bandwidth Limitations in Monolithic 1.3 μm InAs/GaAs Quantum Dot Lasers on Silicon." Journal of Lightwave Technology (2018).

[37] J. Van der Ziel, R. Dupuis, R. Logan, and C. Pinzone, "Degradation of GaAs lasers grown by metalorganic chemical vapor deposition on Si substrates," Appl. Phys. Lett., vol. 51, no. 2, pp. 89–91, 1987.

[38] A. Y. Liu, et al., "Reliability of InAs/GaAs quantum dot lasers epitaxially grown on silicon," IEEE J. Sel. Top. Quantum Electron., vol. 21, no. 6, Nov./Dec. 2015, Art. no. 1900708.

[39] D. Jung, et al., "Impact of threading dislocation density on the lifetime of InAs quantum dot lasers on Si," Applied Physics Letters, vol. 112, no. 15, p. 153507, 2018.

**ALL BIOS ARE REQUIRED IF PAPER IS ACCEPTED**

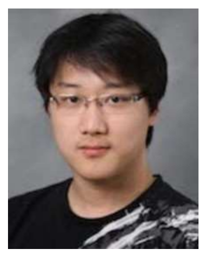

Chen Shang received his B.S. degree in Material Science and Engineering from Purdue University, IN, USA in 2016. He is currently working toward his Ph.D. in Materials at the University of California, Santa Barbara, CA, USA. He is a recipient of Peter J. Frenkel Foundation Fellowship.

His research interests are InAs quantum dots on InP lattice constant for telecom application and low defect density III-V buffer structure grown on Si via molecular beam epitaxy.

Yating Wan received her Ph.D. degree in the Department of Electrical and Computer Engineering from Hong Kong University of Science and Technology, in 2017, for which she had been awarded PhD Research Excellence Award 2016-17. In 2017, she joined Prof. John Bowers' group in University of California Santa Barbara, as a Postdoctoral Research Associate. Her research interests include microcavity quantum dot optoelectronics and silicon photonics.

Justin Norman (S'14–M'18) received B.S. degrees in chemical engineering and physics from the University of Arkansas at Fayetteville, Fayetteville, AR, USA in 2013. He received a Ph.D. in Materials from the University of California, Santa Barbara, CA, USA in 2018 as a National Science Foundation Graduate Research Fellow and a Frenkel Foundation Fellow. He is currently a postdoctoral researcher at the University of California, Santa Barbara.

His research interests are in the growth of InAs quantum dots via molecular beam epitaxy for applications in photonics and quantum electrodynamics. He also works on the heteroepitaxy of III-V materials on Si for photonic integration.

Noelle Collins is currently working toward the Ph.D. degree at the University of California, Santa Barbara, CA, USA. Her research interests include characterization and modeling of quantum dot laser epitaxially grown on silicon as well as passive-active integration of photonic devices with quantum dot active region on monolithic III-V on silicon platform.

Ian MacFarlane, is currently working as a research intern at the University of California, Santa Barbara, CA, USA. His research interests include characterization of quantum dot laser epitaxially grown on silicon as well as passive-active integration of photonic devices with quantum dot active region on monolithic III-V on silicon platform.

Mario Dumont is currently working toward the Ph.D. degree at the University of California, Santa Barbara, CA, USA. Her research interests include characterization and modeling of quantum dot laser epitaxially grown on silicon as well as passive-active integration of photonic devices with quantum dot active region on monolithic III-V on silicon platform.

Songtao Liu received the B.E. (Hons.) degree in electronic information science and technology from Henan University, Kaifeng, China, in 2012 and the Ph.D. degree in microelectronics and solid state electronics from the University of Chinese Academy of Sciences, Beijing, China, 2017. His Ph.D. dissertation was on monolithically integrated InP-based mode-locked lasers.

He is currently a Postdoctoral Researcher at the University of California, Santa Barbara, Santa Barbara, CA, USA. His research interests are in the field of photonic integrated circuits, with an emphasis on monolithically integrated mode locked lasers and tunable lasers both on InP and silicon platform.

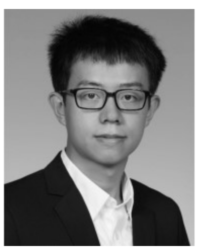

Qiang Li (S'12–M'15) received the B.S. degree from Peking University, Beijing, China, in 2009, and the Ph.D. from The Hong Kong University of Science and Technology, Hong Kong, in 2014. He is currently a lecturer, in School of Physics and Astronomy, Cardiff University. His current research interests include epitaxial integration of III–V high mobility transistors and lasers on silicon substrate by MOCVD

Kei May Lau (S'78–M'80–SM'92–F'01) received the B.S. and M.S. degrees in physics from the University of Minnesota, Minneapolis, in 1976 and 1977, respectively, and the Ph.D. degree in electrical engineering from Rice University, Houston, TX, in 1981. She is currently a Chair Professor with the Department of Electronic and Computer Engineering, Hong Kong University of Science and Technology, Hong Kong. She was on the faculty of the ECE Department at the University of Massachusetts/Amherst before joining HKUST in 2000. Her group's research interests are primarily III–V and wide bandgap semiconductor materials and devices, for integration on silicon.

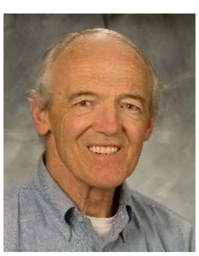

(SM'88–F'01–LF'12) Arthur C. Gossard was born in Ottawa, Illinois in 1935. He received the B.A. degree summa cum laude in physics from Harvard University in Cambridge, Massachusetts in 1956 and the Ph.D. degree in physics from University of California Berkeley in Berkeley, California in 1960.

He was Member of Technical Staff at AT&T Bell Telephone Laboratories from 1960 to 1987. He then became Professor at University of California Santa Barbara in Santa Barbara, CA where he has served from 1987 to the present. His current research interests center on molecular beam epitaxial crystal growth and on the creation and application of artificially structured quantum materials.

Prof. Gossard is a member of IEEE, the American Physical Society and the Materials Research Society. He discovered the first nuclear magnetic resonance in ferromagnets. He also grew the first alternate monolayer superlattices and created the first high mobility modulation doped semiconductors. He co-discovered fractional quantization of the quantum Hall effect and the quantum confined Stark effect. He is a member of both the National Academy of Sciences and the National Academy of Engineering.

John Bowers is Director of the Institute for Energy Efficiency and a professor in the Departments of Electrical and Computer Engineering and Materials at the University of California, Santa Barbara. His research interests are primarily concerned with silicon photonics, optoelectronic devices, optical switching and transparent optical networks and quantum dot lasers. Bowers received the M.S. and Ph.D. degrees from Stanford University and then worked for AT&T Bell Laboratories before joining UCSB. Bowers is a fellow of the IEEE, OSA and the American Physical Society, and a recipient of the IEEE Photonics Award, OSA/IEEE Tyndall Award, the IEEE LEOS William Streifer Award and the South Coast Business and Technology Entrepreneur of the Year Award. He is a member of the National Academy of Engineering and the National Academy of Inventors.